Available online at www.sciencedirect.com
ScienceDirect
Journal of Computational Physics 220 (2006) 394–408
JOURNAL OF COMPUTATIONAL PHYSICS
www.elsevier.com/locate/jcp

Finite element modeling of lipid bilayer membranes

Feng Feng [1], William S. Klug *

Department of Mechanical and Aerospace Engineering, University of California, Los Angeles, CA 90095, United States

Received 20 January 2006; received in revised form 16 May 2006; accepted 17 May 2006
Available online 10 July 2006

Abstract

A numerical simulation framework is presented for the study of biological membranes composed of lipid bilayers based on the finite element method. The classic model for these membranes employs a two-dimensional-fluid-like elastic constitutive law which is sensitive to curvature, and subjects vesicles to physically imposed constraints on surface area and volume. This model is implemented numerically via the use of C^1-conforming triangular Loop subdivision finite elements. The validity of the framework is tested by computing equilibrium shapes from previously-determined axisymmetric shape-phase diagram of lipid bilayer vesicles with homogeneous material properties. Some of the benefits and challenges of finite element modeling of lipid bilayer systems are discussed, and it is indicated how this framework is natural for future investigation of biologically realistic bilayer structures involving nonaxisymmetric geometries, binding and adhesive interactions, heterogeneous mechanical properties, cytoskeletal interactions, and complex loading arrangements. These biologically relevant features have important consequences for the shape mechanics of nonidealized vesicles and cells, and their study requires not simply advances in theory, but also advances in numerical simulation techniques, such as those presented here.

PACS: 87.16.Dg; 87.16.Ac; 02.70.Dh; 46.15.−x; 46.70.Hg

Keywords: Biomembranes; Lipid bilayer mechanics; Cell mechanics; Finite element; Subdivision surfaces

1. Introduction

The lipid bilayer membrane is an ubiquitous structural motif in biology. From the membranes which form the outer boundaries of cells and cell organelles such as the endoplasmic reticulum (ER), the Golgi apparatus, and mitochondria, to the transport vesicles which travel within cells, to the membranes surrounding enveloped viruses such as HIV, lipid bilayers are critical components to a myriad of biological entities. Furthermore, the mechanics of shape and deformation of bilayer membranes is centrally important for their many cellular functions. [1,2]. Unique flexibility is responsible for the striking membrane conformations observed in the tubules

* Corresponding author.
E-mail address: klug@ucla.edu (W.S. Klug).
[1] Present address: ABAQUS East, Providence, RI, USA.

0021-9991/$ - see front matter
doi:10.1016/j.jcp.2006.05.023

and fenestrations of the ER and Golgi [3] and intricate cristae networks of mitochondria [4], as well as for the ability to generate local regions of high curvature in the budding of transport vesicles and viruses [2]. The forces necessary to produce and maintain these membrane configurations are the result of interactions of the membranes with proteins. Similar membrane–protein force interactions govern cell adhesion and the formation of filapodia and lamellapodia for cell motion. Ultimately, a rich understanding of the relationships among force, geometry, and biological function in each of the cases mentioned above will require quantitative physical models which respect the biological complexity of membranes containing of multiple lipid types and intermembrane proteins, and complex membrane and forcing configurations not subject to any artificially imposed symmetry conditions. Theoretical models of this sort will be necessarily coupled to numerical methods of solution, such as those presented in this article. The present work is motivated precisely by the drive to develop more biologically realistic models of membrane mechanics.

Lipid bilayer membranes are composed of amphiphilic lipid molecules which, in an aqueous environment, self-assemble into bilayers which close to form ''pouches'' called vesicles. The two-dimensional fluid-like nature of the lipid monolayers combined with their stiffness in stretching and bending gives the membranes unique mechanical properties of large deformability and the ability to adopt a wide variety of shapes quite unlike any macroscopic materials from which shell structures are typically engineered.

The mechanical energy of lipid bilayers is governed by three significant contributions [1]: bending or curvature of the monolayers; expansion and contraction of the monolayers, i.e. local changes in lipid density; and osmotic pressure. The energy scales of these factors are conveniently seperable with the energies of the last two exceeding that of the first by several orders of magnitude [1]. Thus, a common simplification is employed by modeling the effects of density change and osmotic pressure with effective constraints on the total area and enclosed volume of a membrane. The classic bilayer mechanics theory developed by Canham [5], Helfrich [6], and Evans [7] proposes a lowest-order ''linear elastic'' bending energy which is a quadratic function of the principle curvatures of the surface. The equations of equilibrium for the classic theory, first calculated by Jenkins [8,9], are fourth-order, highly nonlinear, partial differential equations, and are extremely difficult to solve in general. Hence most analytical efforts have focused on solving the simplified equilibrium equations for axisymmetric geometries. Fairly complete phase diagrams have been calculated [10] parameterizing the catalog of stationary vesicle shapes. A few incrementally improved forms of the curvature energy have also been proposed, most notably the so-called Area Difference Elasticity Model (ADE) [11–14] wherein the Canham–Helfrich–Evans energy is supplemented by consideration of curvature-induced area changes in the inner and outer monolayers. The ADE model has been shown to yield a slightly richer set of equilibrium shapes, and has proven more adept at explaining accurately phenomena such as tethering [13].

For nonaxisymmetric membrane geometries, the equations of equilibrium are not amenable to direct solution. One alternative is to minimize the curvature energy over a reduced subspace of membrane configurations. In the style of a Rayleigh–Ritz procedure, the surface of a vesicle can be approximated as a linear combination of a set of pre-selected basis functions, and the function weights adjusted to minimize the energy [5,15,16]. Another alternative approach is to sum discrete finite-difference curvature approximations on a triangulated net, forming a discrete version of the energy, which is then minimized often by a conjugate gradient algorithm. Variants of this approach have been taken by a number of researchers [e.g. [17–20]], some using the free software package Surface Evolver by Brakke [21]. Bloor and Wilson [22] have developed a method based on solution of elliptical PDEs which they have shown to be very efficient for computing nonaxisymmetric equilibrium membrane shapes. Du et al. [23,24] have developed a phase-field method which is capable of computing nonaxisymmetric equilibrium shapes, and is the only method available which can simulate changes in membrane topology.

It is noteworthy that both the direct variational and discrete triangulation approaches bear some resemblance to the finite element method [25]. However, very little exists in the literature regarding finite element treatment of lipid bilayer mechanics. In one related study, Dao et al. [26] modeled the red blood cell with finite elements focusing on the mechanics of the cytoskeletal spectrin network which dominates the deformation energy, allowing the bilayer to be neglected.

The finite element method (FEM) can, in fact, be viewed as a hybrid of the Ritz method and the discrete methods mentioned above. In the context of lipid bilayer mechanics, the local support of the FE basis

functions is particularly useful, enabling straightforward local application of external loads and/or constraints, and allowing for arbitrarily complex geometries. Furthermore, the numerical convergence properties of FEM are known to be much better than those of local finite-difference techniques [27], which have retained the most popularity for previous numerical work on bilayers.

Since the bending energy is a quadratic functional of the curvatures, the space of admissible trial functions is H^2, i.e. the space of square-integrable surface functions having square integrable derivatives through second-order [27]. Roughly, this is consistent with surfaces which are C^1, i.e. having continuous first derivatives. This requirement, which also applies to the mechanics of thin shells as modeled by Kirchhoff–Love shell theory, has traditionally proven quite difficult to satisfy. As a result, most shell finite elements are formulated to satisfy the C^1 constraint only approximately or via alternative shell theories which do not depend on curvature. The recent development of C^1-conforming thin-shell finite elements based on the method of subdivision surfaces [28,29] created for computer graphics applications has provided a robust alternative to the modified formulations.

The main objective of this work is development of a finite element framework for simulation of the mechanical deformation and equilibrium of lipid bilayer membranes. Toward this objective, C^1-conforming subdivision finite elements are employed to represent membrane geometry, and the classic Canham–Helfrich–Evans model of bilayer bending energy is combined with global constraints on membrane area and enclosed volume to form a discrete energy minimization problem. Effectiveness of the FE framework is demonstrated through the calculation of equilibrium shapes for several combinations of prescribed vesicle area and volume, results which are validated by comparison to axisymmetric calculations found in the literature. In carrying out these calculations some subtle but important issues emerge pertaining to the enforcement of area constraints, use of numerical quadrature, and the need for stabilization of tangential nodal motions. Strategies are developed to deal with these issues. Though ultimately it is desirable to extend the FE framework for more complex bilayer modeling, the present work considers membranes with uniform material properties, subject to no external forces other than the pressure implicit with the constraint on volume.

By way of outline, this paper continues in Section 2 with the variational formulation of equilibrium for the classic Canham–Helfrich–Evans bilayer mechanics model, along with a discussion of strategies for enforcing global constraints on membrane area and enclosed volume. Section 3 formulates the finite element discretization of the variational membrane mechanics problem. Section 4 presents the calculation of constrained equilibrium shapes validating results against previous work from the literature. Section 5 concludes with discussion of results and thoughts about future development and applications.

2. Lipid bilayer mechanics

As noted above, a lipid bilayer membrane can be described mechanically as a deformable fluid surface. Inextensibility of this surface and its inability to sustain local shear stress leave bending as the most significant mode of deformation, with the strain energy of the membrane depending on the curvatures of the surface. Balance of osmotic pressure across the membrane surface also fixes the volume enclosed within a vesicle, and thus equilibrium shapes of vesicles are minimal bending energy surfaces which respect equality constraints on area and volume. Seifert [1] provides an good introduction to the formulation of models for bilayer shape mechanics and a thorough review of the related literature. Here the geometry and kinematics of surfaces are reviewed briefly after which the bilayer energy is introduced and the variational problem formulated in a weak form suitable for approximation by the finite element method.

2.1. Kinematics

The bilayer membrane is described as a two-dimensional surface embedded in three-dimensional space. Details regarding the geometry of surfaces can be found in any of the standard texts on differential geometry (e.g. [30,31]). Let $\mathscr{M}$ represent a membrane surface, parameterized by curvilinear coordinates $\{s^1, s^2\}$, such that its position vector $\boldsymbol{x} \in \mathbb{R}^3$ is given by the map $\boldsymbol{x} = \boldsymbol{x}(s^1, s^2)$, as depicted in Fig. 1. The (covariant) basis vectors corresponding to the curvilinear coordinates (s^α) are

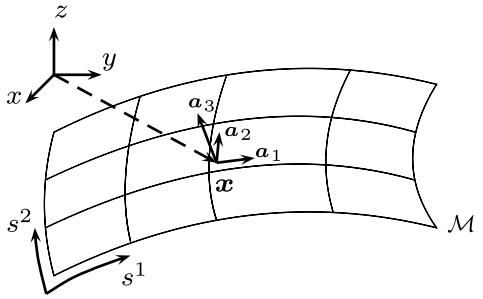

Fig. 1. Geometry of a surface.

$$\boldsymbol{a}_\alpha = \frac{\partial \boldsymbol{x}}{\partial s^\alpha} \equiv \boldsymbol{x}_{,\alpha}. \tag{1}$$

The summation convention is implied with Greek indices taking values of 1 and 2, and comma is used to denote partial differentiation with respect to the surface coordinates. For later reference, the dual (contravariant) basis vectors $\boldsymbol{a}^\alpha$ are defined such that $\boldsymbol{a}^\alpha \cdot \boldsymbol{a}_\beta = \delta^\alpha_\beta$. The covariant and contravariant components of the surface metric tensor in turn follow as

$$a_{\alpha\beta} = \boldsymbol{a}_\alpha \cdot \boldsymbol{a}_\beta, \qquad a^{\alpha\beta} = \boldsymbol{a}^\alpha \cdot \boldsymbol{a}^\beta, \tag{2}$$

respectively. The infinitesimal element of area over the surface $\mathscr{M}$ at point (s^1, s^2) is then

$$dS = \sqrt{a} ds^1 ds^2 \equiv \sqrt{a} d^2 s, \tag{3}$$

where $\sqrt{a}$ is the surface measure and a is the determinant of the covariant metric tensor $a = |a_{\alpha\beta}|$. The shell director $\boldsymbol{d} \equiv \boldsymbol{a}_3$, defined as the unit normal to the surface, has the properties

$$\boldsymbol{a}_\alpha \cdot \boldsymbol{a}_3 = 0 \qquad |\boldsymbol{a}_3| = 1, \tag{4}$$

and the explicit form

$$\boldsymbol{d} \equiv \boldsymbol{a}_3 = \frac{\boldsymbol{a}_1 \times \boldsymbol{a}_2}{|\boldsymbol{a}_1 \times \boldsymbol{a}_2|} = \frac{\boldsymbol{a}_1 \times \boldsymbol{a}_2}{\sqrt{a}}. \tag{5}$$

The symmetric curvature tensor $\mathbf{B}$ is defined having covariant components

$$b_{\alpha\beta} = -\boldsymbol{d}_{,\alpha} \cdot \boldsymbol{a}_\beta = \boldsymbol{d} \cdot \boldsymbol{a}_{\alpha,\beta} = b_{\beta\alpha}. \tag{6}$$

Bilayer mechanics is most naturally described in terms of two invariants of the curvature tensor, the mean curvature and Gaussian curvature. The mean curvature is one half of the trace of the curvature tensor

$$H = \frac{1}{2}\mathrm{tr}(\mathbf{B}) = \frac{1}{2} b^\alpha_\alpha = -\frac{1}{2} \boldsymbol{a}^\alpha \cdot \boldsymbol{d}_{,\alpha}, \tag{7}$$

and the Gaussian curvature is the determinant of the curvature tensor

$$K = \det(\mathbf{B}) = |b^\alpha_\beta|. \tag{8}$$

2.2. Energy and the variational problem

To lowest order, the bending energy of the membrane is quadratic in the curvatures, and may be written

$$E[\boldsymbol{x}] = \int_{\mathscr{M}} \left[\frac{1}{2} \mathscr{K}_C (2H - C_0)^2 + \mathscr{K}_G K \right] \sqrt{a} \mathrm{d}^2 s. \tag{9}$$

Here $\mathscr{K}_C$ and $\mathscr{K}_G$ are the bending modulus and Gaussian saddle-splay modulus, respectively, and C_0 is the so-called *spontaneous curvature* which reflects any initial or intrinsic curvature of the membrane. Spontaneous curvature may be nonzero due, for example, to splayed geometry of individual lipids; however, such

effects are often mitigated by the slow process of flipping of lipids from one layer to the other [1]. If the Gaussian modulus is uniform over a membrane surface of fixed topology with genus g, then the Gaussian curvature integrates to a constant $\int_{\mathscr{M}} K \mathrm{d}A = 4\pi(1-g)$ by the Gauss–Bonnet theorem [30]. In this case, the Gaussian term in (9) is topologically invariant and its first variation is identically zero, such that this term has no effect on the resulting equilibrium equations. Here this is assumed to be the case. It is notable that since its effect is absent from the governing equations, the Gaussian modulus has eluded direct measurement. The model developed from the energy (9) is attributed to Canham, Helfrich and Evans, who introduced it independently [5–7].

If a membrane is under the influence of a conservative external load with potential V^{ext}, such that $\Pi[\boldsymbol{x}] \equiv E[\boldsymbol{x}] + V^{\mathrm{ext}}[\boldsymbol{x}]$ is the total potential energy, then according to the principle of minimum potential energy, stable equilibrium configurations follow as minimizers of Π. Nonconservative loads can also be considered variationally via the principle of virtual work; however, here minimum potential energy is invoked to provide a simple and clear framework for enforcing global constraints on area and volume. As noted above, energy minimization must be effected in the presence of global constraints on the total area and enclosed volume of the membrane. For fixed total area $\bar{A}$ and enclosed volume $\overline{V}$, we denote the space of admissible membrane configurations as

$$H^2_{AV}(\mathscr{M}) = \{\boldsymbol{x} : \boldsymbol{x} \in H^2(\mathscr{M}), A[\boldsymbol{x}] = \bar{A}, V[\boldsymbol{x}] = \overline{V}\}, \tag{10}$$

where $A[\boldsymbol{x}]$ is the total area and $V[\boldsymbol{x}]$ is the enclosed volume of the membrane with shape $\boldsymbol{x}$, and $H^2(\mathscr{M})$ is the Sobolev space of square-integrable functions having square-integrable partial derivatives through second-order. In other words, the space of admissible trial functions is the subspace of $H^2(\mathscr{M})$ the members of which satisfy the area and volume constraints. Therefore the constrained minimization problem for equilibrium membrane configurations may be written

$$\min_{\boldsymbol{x} \in H^2_{AV}(\mathscr{M})} \Pi[\boldsymbol{x}]. \tag{11}$$

For most areas and volumes this problem exhibits a lack of convexity which is manifested in the existence of multiple equilibrium shapes. One of the benefits of the energy minimization framework is that the energies of these local minima can easily be compared to evaluate the relative likelihood of their physical realization. Given that membrane bending energies are typically a couple of orders of magnitude larger than $k_B T$ [1] it is reasonable to expect that thermodynamic equilibrium shapes will be global minimizers. This has in fact been born out by experimental evidence indicating the dominance of global energy minimizers over higher-energy local minimizers [1].

2.2.1. Constraints

The governing equilibrium equations for (9) were first derived by Jenkins [8,9] as the Euler–Lagrange equations of (11) using Lagrange multipliers to satisfy constraints. Enforcement of constraints with multipliers in the context of direct variational methods (such as FEM) has the awkward consequence of changing the minimization problem (11) to a saddle-point problem which can be more difficult to handle numerically. Thus, a penalty approach [32,33] is followed in this work, to approximate the constrained minimization problem (11) as an unconstrained minimization problem by adding terms to the potential energy functional which penalize violations of the two constraints

$$\min_{\boldsymbol{x} \in H^2(\mathscr{M})} I[\boldsymbol{x}], \tag{12a}$$

$$I[\boldsymbol{x}] = \Pi[\boldsymbol{x}] + \frac{\mu_{\mathrm{s}}}{2}(A[\boldsymbol{x}] - \bar{A})^2 + \frac{\mu_{\mathrm{v}}}{2}(V[\boldsymbol{x}] - \overline{V})^2, \tag{12b}$$

where μ_{s} and μ_{v} are arbitrarily large positive numbers chosen to enforce the constraints to within a desired precision.

An important feature of both the original (9) and modified (12b) energy functionals is that the dependence on the surface map $\boldsymbol{x}(s^1, s^2)$ is invariant upon changes in parameterization [34]. In other words, these functionals depend on the shape of the membrane surface, but not on the coordinate parameterization of the shape. From the perspective of continuum mechanics, parameterization invariance of the bilayer energy

is associated with the lack of a well-defined *reference configuration*, mapping the individual lipids to reference positions in space. This feature is not shared by solid shells, the materials of which are sensitive to in-plane tensile, compressive, and shearing deformations which expressed locally in terms of first derivatives of the surface position map as parameterized in both the reference and deformed configurations. Local stretching and shearing of the deformed parameterization of a bilayer is not physically relevant since it cannot be meaningfully compared to a reference parameterization. This is an important consequence of the fact that lipids can flow on the deformed membrane surface, in turn enabling the bilayer to accommodate extreme shape changes inaccessible by solid shells. One important result is that bilayer membranes are only able to support external forces applied in the direction normal to the surface, and not tangentially applied forces.

In light of the bilayer energy's parameterization invariance, one convenient and slight modification of (12b) involves exchanging the global area constraint for a local one. Since tangential motions of individual material points are not tracked within the fluid bilayer, local and global incompressibility are equivalent. Since the total area is given by $A[\boldsymbol{x}] = \int_{\mathscr{M}} \sqrt{a}\mathrm{d}^2 s$ the area constraint can be enforced locally by penalizing changes in the local surface measure

$$I[\boldsymbol{x}] = \Pi[\boldsymbol{x}] + \frac{\mu_s}{2}\int_{\mathscr{M}} (\sqrt{a} - \sqrt{\bar{a}})^2 \mathrm{d}^2 s + \frac{\mu_v}{2}(V - \overline{V})^2, \tag{12c}$$

where $\sqrt{\bar{a}}$ is some (any) measure for which $\bar{A} = \int_{\mathscr{M}} \sqrt{\bar{a}}\mathrm{d}^2 s$. This local penalty functional is employed in the subsequent development to aid in stabilizing tangential motions of finite element nodes on the meshed surface.

2.2.2. Weak form

In this variational context, the finite element approach avoids direct use of the membrane equilibrium equations, i.e. the strong form of the equilibrium statement, and rather discretizes the weak form obtained from the first variation of the energy, as formulated here. For arbitrary admissible variations of the membrane surface $\delta\boldsymbol{x} \in H^2(\mathscr{M})$, the first variation of the total potential energy functional is

$$\begin{aligned}\delta\Pi &= \delta\int_{\mathscr{M}} \mathscr{K}_C \frac{1}{2}(2H - C_0)^2\sqrt{a}\mathrm{d}^2 s + \delta V^{\mathrm{ext}} \\ &= \int_{\mathscr{M}} \left[\mathscr{K}_C 2(2H - C_0)\delta H\sqrt{a} + \mathscr{K}_C \frac{1}{2}(2H - C_0)^2\delta\sqrt{a}\right]\mathrm{d}s^1\mathrm{d}s^2 - \int_{\mathscr{M}} \boldsymbol{f}^{\mathrm{ext}}\cdot\delta\boldsymbol{x}\sqrt{a}\mathrm{d}^2 s,\end{aligned}$$

where $\boldsymbol{f}^{\mathrm{ext}}$ is a conservative external force distributed over the membrane surface. The variations of the surface measure and mean curvature are easily computed as,

$$\begin{aligned}\delta\sqrt{a} &= \sqrt{a}\boldsymbol{a}^\alpha\cdot\delta\boldsymbol{a}_\alpha, \\ \delta H &= -\frac{1}{2}\boldsymbol{a}^\alpha\cdot(\delta\boldsymbol{d})_{,\alpha} + \frac{1}{2}a^{\alpha\beta}\boldsymbol{d}_{,\alpha}\cdot\delta\boldsymbol{a}_\beta,\end{aligned}$$

such that $\delta\Pi$ can be written

$$\delta\Pi = \int_{\mathscr{M}} \left\{\left[\mathscr{K}_C(2H - C_0)a^{\alpha\beta}\boldsymbol{d}_{,\alpha} + \mathscr{K}_C\frac{1}{2}(2H - C_0)^2\boldsymbol{a}^\beta\right]\cdot\delta\boldsymbol{a}_\beta - \mathscr{K}_C(2H - C_0)\boldsymbol{a}^\alpha\cdot(\delta\boldsymbol{d})_{,\alpha} - \boldsymbol{f}^{\mathrm{ext}}\cdot\delta\boldsymbol{x}\right\}\sqrt{a}\mathrm{d}^2 s,$$

or more concisely,

$$\delta\Pi = \int_{\mathscr{M}} [\boldsymbol{n}^\alpha\cdot\delta\boldsymbol{a}_\alpha + \boldsymbol{m}^\alpha\cdot\delta\boldsymbol{d}_{,\alpha} - \boldsymbol{f}^{\mathrm{ext}}\cdot\delta\boldsymbol{x}]\sqrt{a}\mathrm{d}^2 s, \tag{13}$$

where stress and moment resultants, $\boldsymbol{n}^\alpha$ and $\boldsymbol{m}^\alpha$, respectively, have been defined as

$$\boldsymbol{n}^\alpha = \mathscr{K}_C(2H - C_0)a^{\alpha\beta}\boldsymbol{d}_{,\beta} + \mathscr{K}_C\frac{1}{2}(2H - C_0)^2\boldsymbol{a}^\alpha \tag{14a}$$

and

$$\boldsymbol{m}^\alpha = -\mathscr{K}_C(2H - C_0)\boldsymbol{a}^\alpha. \tag{14b}$$

The first variation of the penalty-modified energy functional (12c) can then be formed as

$$\delta I = \delta \Pi + \mu_s \int_{\mathscr{M}} (\sqrt{a} - \sqrt{\bar{a}}) \delta \sqrt{a} \mathrm{d}^2 s + \mu_v (V - \overline{V}) \delta V.$$

By the divergence theorem, the volume can be written

$$V = \int_V \mathrm{d}V = \int_V \frac{1}{3} \nabla \cdot \boldsymbol{x} \, \mathrm{d}V = \frac{1}{3} \int_{\mathscr{M}} \boldsymbol{x} \cdot \boldsymbol{d} \sqrt{a} \mathrm{d}^2 s,$$

and thus its variation is

$$\delta V = \frac{1}{3} \int_{\mathscr{M}} [\boldsymbol{d} \cdot \delta \boldsymbol{x} + \boldsymbol{x} \cdot \delta \boldsymbol{d} + (\boldsymbol{x} \cdot \boldsymbol{d}) \boldsymbol{a}^\alpha \cdot \delta \boldsymbol{a}_\alpha] \sqrt{a} \mathrm{d}^2 s = \frac{1}{3} \int_{\mathscr{M}} \{\boldsymbol{d} \cdot \delta \boldsymbol{x} + [(\boldsymbol{x} \cdot \boldsymbol{d}) \boldsymbol{a}^\alpha - (\boldsymbol{x} \cdot \boldsymbol{a}^\alpha) \boldsymbol{d}] \cdot \delta \boldsymbol{a}_\alpha\} \sqrt{a} \mathrm{d}^2 s.$$

δI can then be written as

$$\delta I = \int_{\mathscr{M}} \left[\hat{\boldsymbol{n}}^\alpha \cdot \delta \boldsymbol{a}_\alpha + \boldsymbol{m}^\alpha \cdot \delta \boldsymbol{d}_{,\alpha} - \hat{\boldsymbol{f}}^{\mathrm{ext}} \cdot \delta \boldsymbol{x} \right] \sqrt{a} \mathrm{d}^2 s, \tag{15a}$$

where $\hat{\boldsymbol{n}}^\alpha$ and $\hat{\boldsymbol{f}}^{\mathrm{ext}}$ are effective stress resultants and an effective external force, modified to include terms from the area and volume constraints

$$\hat{\boldsymbol{n}}^\alpha = \boldsymbol{n}^\alpha + \mu_s (\sqrt{a} - \sqrt{a_0}) \boldsymbol{a}^\alpha + \frac{\mu_v (V - \overline{V})}{3} [(\boldsymbol{x} \cdot \boldsymbol{d}) \boldsymbol{a}^\alpha - (\boldsymbol{x} \cdot \boldsymbol{a}^\alpha) \boldsymbol{d}], \tag{15b}$$

$$\hat{\boldsymbol{f}}^{\mathrm{ext}} = \frac{\mu_v (V - \overline{V})}{3} \boldsymbol{d} - \boldsymbol{f}^{\mathrm{ext}}. \tag{15c}$$

The condition for equilibrium in the weak form is stationarity of the energy functional, $\delta I = 0$. Integration by parts of the terms involving $\delta \boldsymbol{a}^\alpha$ and $\delta \boldsymbol{d}_{,\alpha}$ would yield the equilibrium (Euler–Lagrange) equations. These local or point-wise equations of equilibrium relate derivatives (up to fourth-order) of the position $\boldsymbol{x}$ to the externally applied load. The finite element approach avoids direct involvement of the local equilibrium equations, by introducing approximations of the fundamental unknown field $\boldsymbol{x}$ into the weak form (15). In particular, this field along with the corresponding test functions $\delta \boldsymbol{x}$ are restricted to a discrete subspace of functions defined by the finite element approximation as introduced in the following section.

3. Ritz-style finite element approximation

Following the Ritz strategy, the minimization problem (12a) is replaced by an approximate problem, minimizing the energy functional $I[\boldsymbol{x}]$ over a finite-dimensional subspace $U_h \subset U$, where $U = H^2(\mathscr{M})$ is the full space of admissible solutions; i.e.

$$\min_{\boldsymbol{x}_h \in U_h} I[\boldsymbol{x}_h]. \tag{16}$$

Letting $\{N_a(s^1, s^2), a = 1, \ldots, \mathscr{N}\}$ be a basis spanning U_h, the Ritz trial functions $\boldsymbol{x}_h$ can be written as linear combinations of basis – or *shape* – functions N_a,

$$\boldsymbol{x}_h(s^1, s^2) = \sum_{a=1}^{\mathscr{N}} \boldsymbol{x}_a N_a(s^1, s^2). \tag{17}$$

The approximate minimization problem (16) then becomes an algebraic minimization problem for the weighting coefficients $\boldsymbol{x}_a \in \mathbb{R}^3$,

$$\min_{\mathbf{x} \in \mathbb{R}^{3\mathscr{N}}} I_h(\mathbf{x}), \tag{18}$$

where $\mathbf{x}^{\mathrm{T}} = \{\boldsymbol{x}_1^{\mathrm{T}}, \ldots, \boldsymbol{x}_{\mathscr{N}}^{\mathrm{T}}\}$ and $I_h(\mathbf{x}) = I[\boldsymbol{x}_h]$. The stationarity condition for $I_h(\mathbf{x})$ can be obtained by substituting (17) into the weak form (15) along with Ritz test functions

$$\delta \boldsymbol{x}_h(s^1, s^2) = \sum_{a=1}^{\mathscr{N}} \delta \boldsymbol{x}_a N_a(s^1, s^2). \tag{19}$$

The arbitrariness of the test weights $\delta \boldsymbol{x}_a$ leads to a set of nonlinear algebraic equations representing the balance of generalized forces work-conjugate to the Ritz coefficients,

$$\boldsymbol{f}_a = \frac{\partial I_h}{\partial \boldsymbol{x}_a} = \int_{\mathscr{M}} \left[\hat{\boldsymbol{n}}^\alpha \cdot \frac{\partial \mathbf{a}_\alpha}{\partial \boldsymbol{x}_a} + \boldsymbol{m}^\alpha \cdot \frac{\partial \boldsymbol{d}_{,\alpha}}{\partial \boldsymbol{x}_a} - \hat{\boldsymbol{f}}^{\text{ext}} N_a \right] \sqrt{a} \mathrm{d}^2 s = 0. \tag{20}$$

The following identities can easily be shown to hold

$$\frac{\partial \boldsymbol{a}_\alpha}{\partial \boldsymbol{x}_a} = N_{a,\alpha} \mathbf{1},$$
$$\frac{\partial \boldsymbol{d}_{,\alpha}}{\partial \boldsymbol{x}_a} = \left(-N_{a,\beta}[\boldsymbol{a}^\beta \otimes \boldsymbol{d}]\right)_{,\alpha} = -N_{a,\beta\alpha}[\boldsymbol{a}^\beta \otimes \boldsymbol{d}] - N_{a,\beta}[\boldsymbol{a}^\beta_{,\alpha} \otimes \boldsymbol{d}] - N_{a,\beta}[\boldsymbol{a}^\beta \otimes \boldsymbol{d}_{,\alpha}],$$

such that the resultant generalized forces are, more explicitly,

$$\boldsymbol{f}_a = \int_{\mathscr{M}} \left[\hat{\boldsymbol{n}}^\alpha N_{a,\alpha} - \boldsymbol{m}^\alpha \cdot \left(N_{a,\beta}[\boldsymbol{a}^\beta \otimes \boldsymbol{d}]\right)_{,\alpha} - \hat{\boldsymbol{f}}^{\text{ext}} N_a \right] \sqrt{a} \mathrm{d}^2 s.$$

The Hessian or tangent stiffness of the energy, which is useful for Newton-type minimization algorithms, can be computed by a second differentiation of the residual nodal forces, $\mathbf{k}_{ab} = \frac{\partial \boldsymbol{f}_a}{\partial \boldsymbol{x}_b}$. However, in the present work this calculation is omitted, as energy minimization calculations employ a nonlinear conjugate gradient solver which does not require the Hessian.

The greatest challenge in carrying out a Ritz procedure lies in the choice of an appropriate basis set $\{N_a\}$ which provides desirable approximation properties as well as efficient numerical evaluation. The finite element flavor of the Ritz method excels in both of these regards by defining interpolating polynomial basis functions with local support over small polygonal subdomains(elements) in an unstructured mesh. Historically, construction of C^1-conforming FE interpolants has proven extremely awkward, requiring the incorporation of nodal values of higher derivatives of the unknown field into the interpolation formula (17) [27]. The demand for C^1 elements in engineering plate and shell analysis has motivated a variety of approaches all attempting to work around the C^1 requirement, either by approximating it or by resorting to Reissner–Mindlin thick-shell theories which require only C^0 interpolation. Recently however, the method of subdivision surfaces has dealt with the C^1 requirement in an exact way, while also avoiding the use of nodal derivatives.

3.1. Subdivision thin shell finite elements

The method of subdivision surfaces, which is popular for modeling of smooth surfaces in computer graphics and geometric design [35], has been established recently [28,29] as a general paradigm for finite element analysis of thin shells in engineering. The triangular subdivision shell finite elements developed in [28,29] based on the Loop subdivision scheme [36] address the C^1 requirement by relaxing the properties of strict interpolation and locality. As discussed in detail in [28] and demonstrated graphically in Fig. 2(a), the subdivision shape function for a node of the triangular mesh has support which extends not just over the triangles connected to the node, but also to adjacent triangles. It can also be seen that the computational (limit) surface is *approximating* rather than *interpolating* as it does not pass through the nodal points, but rather defines a smooth surface approximating the control mesh.

Each subdivision shape function has a support which covers not only the triangular elements connected to the corresponding node, but also next-nearest-neighbor elements. As a consequence, the domain of an individual element e coincides with the support of shape functions in the *one-ring* of $\mathscr{N}_e$ control mesh vertices connected to e and elements adjacent to e (see Fig. 2(b)). Thus the Ritz approximation of the membrane surface can be evaluated over the domain of a triangular element e in terms of the nodal positions and shape functions of its *one-ring*,

$$\boldsymbol{x}_h(s^1, s^2) = \sum_{a=1}^{\mathscr{N}_e} \boldsymbol{x}_a N_a(s^1, s^2). \tag{21}$$

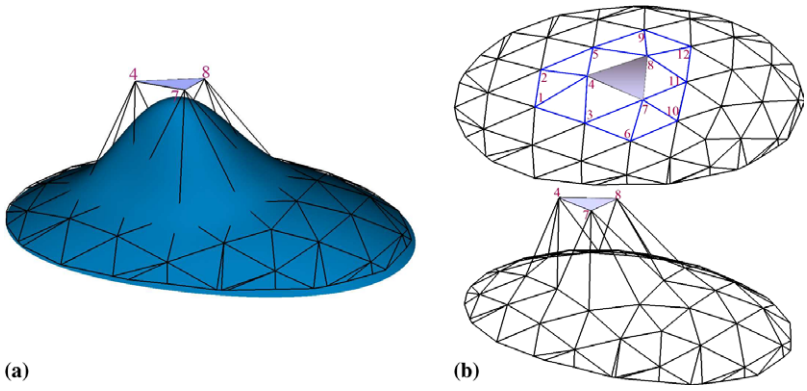

Fig. 2. C^1 Loop subdivision shell elements. (a) C^1 limit surface (blue) approximating a control mesh (black). (Details regarding the precise analytical form of the subdivision shape functions and evaluation of the limit surface are found in [28].) (b) The one-ring of vertices (numbered) surrounding a typical element. The domain of the center element overlaps with the shape functions of (one-ring) vertices connected to element and adjacent elements. (For interpretation of reference to colour in this figure legend, the reader is refered to the web version of this article.)

The energy, area, volume, and force integrals are summed over the entire membrane surface. As the surface domain is discretized by a finite element mesh, integrals are computed as the sums of single-element contributions, each of which is an integral over the domain of an individual element. For example, the nodal forces (20) are evaluated in pieces over the element domains $\mathscr{M}_e, e = 1, \ldots, \mathscr{E}$ and summed as

$$\boldsymbol{f}_a = \sum_{e=1}^{\mathscr{E}} \boldsymbol{f}_a^e; \quad \boldsymbol{f}_a^e = \int_{\mathscr{M}_e} \left(\hat{\boldsymbol{n}}^\alpha \cdot \frac{\partial \boldsymbol{a}_\alpha}{\partial \boldsymbol{x}_a} + \boldsymbol{m}^\alpha \cdot \frac{\partial \boldsymbol{d}_{,\alpha}}{\partial \boldsymbol{x}_a} - \hat{\boldsymbol{f}}^{\text{ext}} N_a \right) \sqrt{a} \, \mathrm{d}^2 s.$$

3.2. Numerical quadrature

In practice, the element integrals are approximated by numerical quadrature. For instance, the contribution of a single generic element to the residual force at node a is computed as

$$\boldsymbol{f}_a^{\text{int}} = -\sum_{p=1}^{\mathscr{Q}} \left[\left(\hat{\boldsymbol{n}}^\alpha \cdot \frac{\partial \boldsymbol{a}_\alpha}{\partial \boldsymbol{x}_a} + \boldsymbol{m}^\alpha \cdot \frac{\partial \boldsymbol{d}_{,\alpha}}{\partial \boldsymbol{x}_a} - \hat{\boldsymbol{f}}^{\text{ext}} N_a \right) \sqrt{a} \right]_{(s_p^1, s_p^2)} w_p, \tag{22}$$

where (s_p^1, s_p^2) are the parametric coordinates of the quadrature points in the element, w_p is the corresponding quadrature weight, and $\mathscr{Q}$ is the number of quadrature points. For convenience in applying the quadrature rule, the barycentric coordinates of each triangular element may be chosen as the covariant surface coordinates (s_p^1, s_p^2). Clearly an element will only have a contribution to the residual force at node a if the support of the shape function N_a extends to the triangular domain of the element. One of the most convenient features of the finite element method is the fact that the shape functions have *local* support, i.e. their support extends to a neighborhood of node a containing the domains of only a few elements. For standard finite element shape functions, that neighborhood contains only the elements adjacent or connected to node a. For the shape functions used in this work, the neighborhood contains adjacent elements and elements in the one-ring surrounding those adjacent elements, as discussed above.

For engineering materials in [28,29], it has been shown that first-order (one-point per element) Gaussian quadrature is sufficient to obtain theoretical convergence rates and high accuracy. However, in the context of bilayer mechanics, this is not trivially the case. In contrast to shells of traditional engineering materials which are sensitive not only to bending, but also to shearing and stretching deformations, bilayer strain energy is dependent only on the mean curvature of the membrane surface. Evaluation of the bilayer energy with one-point quadrature results in the emergence of spurious, zero-energy, deformation modes for the finite element mesh. Eigenvalue analysis and numerical experiments confirm that these modes are consequences of the insensitivity of the membrane energy to dilatational and shearing deformations. In particular, many of these modes

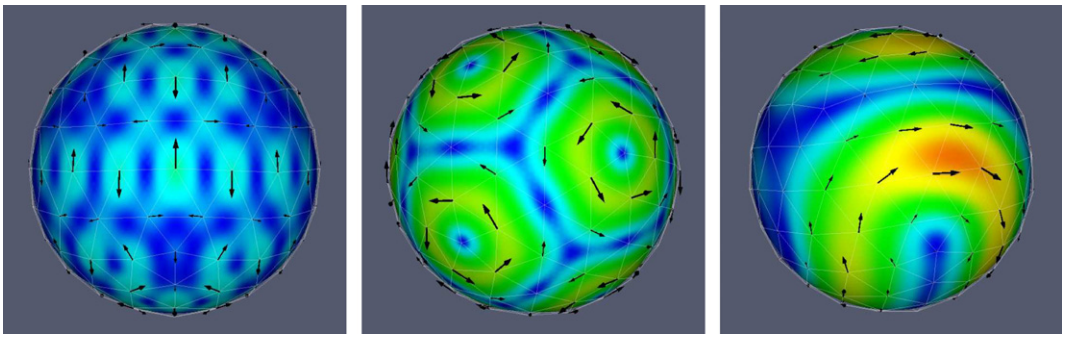

Fig. 3. Spurious shear-like zero-energy modes on a spherical vesicle under-integrated with one-point quadrature. Arrows and color indicate nodal displacements given by eigenvectors corresponding to zero eigenvalues of the stiffness matrix (computed by numerical differentiation of the residual forces). The deformations indicate shear-like "flow" of the nodes on the surface of the vesicle. (For interpretation of reference to colour in this figure legend, the reader is refered to the web version of this article.)

are suppressed by enforcing the area constraint locally via Eq. (12c) as discussed above; however, the spurious shear-like modes can not be completely stabilized in this way. Numerical experiments have shown that evaluation of the locally penalized energy (12c) with one quadrature point per element does indeed produce a non-positive-definite stiffness, and multiple unstable spurious modes, most of which can be easily interpreted as shearing deformations as shown in Fig. 3. Fortunately, the situation is somewhat improved through the use of second-order (three-point) Gaussian quadrature. Numerical experiments reveal that fewer spurious modes are present with the three-point rule, and that those remaining are not easily excited in a typical analysis. For this work, simulations have been performed minimizing the total energy via iterative nonlinear conjugate gradient (CG) methods [33]. Since the stiffness matrix is not required by the nonlinear CG algorithm, its singularity does not prevent solution of the equilibrium equations; however, it does slow the solution process as the solver is required to explore an energy landscape which is flat in the directions defined by the spurious modes. In this respect, efficiency is largely dependent on the sophistication of the line search technique employed by the CG method. A line search algorithm satisfying the strong Wolfe conditions described in Nocedal and Wright [33] has provided robust performance in the present calculations. In addition, numerical techniques using viscous regularization are currently being investigated for their ability to speed up the solution process.

4. Example – shape vs. reduced volume

In this section, the results of a series of numerical simulations are presented to verify and validate the present finite element method for bilayer membrane mechanics. These simulations were carried out by nonlinear conjugate gradient minimization of the energy functional (12c) discretized with susbdivision shell finite elements as discussed in Section 3. Local enforcement of the area constraint is combined with a three-point quadrature rule for numerical integration in order to stabilize spurious zero-energy deformation modes.

Even under the simplest conditions possible, in the absence of any externally applied force, bilayer vesicles exhibit rich mechanical behavior. The two constraints on area and volume conspire together to yield a variety of energy minimizing vesicle shapes as observed in nature. A quick inspection of the Canham–Helfrich–Evans energy (9) notes that the quantity $\int_{\mathscr{M}} H^2 \mathrm{d}A$ is dimensionless, indicating that for $C_0 = 0$ the energy is *scale-invariant*. As a result, the "phase-space" of equilibrium shapes under zero external force, can be parameterized by two-dimensionless numbers, the *reduced spontaneous curvature*, c_0, and the *reduced volume* v, defined by

$$c_0 = C_0 R_0, \quad v = \frac{V}{(4\pi/3)R_0^3}, \tag{23}$$

where $R_0 = \sqrt{A/4\pi}$ is the radius of a sphere with the area A of the vesicle. Rewriting these in terms of A gives

$$c_0 = C_0 \sqrt{\frac{A}{4\pi}}, \quad v = \frac{6\sqrt{\pi}V}{A^{3/2}}.$$

The reduced volume is the ratio of the current volume of the vesicle and the maximum volume that the current total area of the membrane can ensphere. For example, a fully inflated, spherical vesicle of area $A = 4\pi R_0^2$ has volume $V = \frac{4}{3}\pi R_0^3$ and reduced volume $v = 1$, whereas a completely collapsed vesicle of the same area has volume $V = 0$ and reduced volume $v = 0$. For values $0 < v < 1$, a vesicle is partially under-inflated, and the resulting shape(s) are determined by equilibrium, i.e. minimization of the Canham–Helfrich–Evans energy. The library of axisymmetric equilibrium shapes corresponding to different choices of reduced volume and spontaneous curvature has been mapped out in a shape phase diagram [10]. At present, the only *nonaxisymmetric* shapes to be been identified as minimizers of the Canham–Helfrich–Evans model energy are shapes of nonspherical topology (e.g. [24,37]).

For the current work, spontaneous curvature is taken to be zero, and the finite element method is used to simulate equilibrium at several values of reduced volume. For each choice of reduced volume, the CG relaxation starts from roughly spherical original mesh, shown in Fig. 5(a), which has a reduced volume of approximately one (not exactly one because the polynomial FE approximation is incapable of representing a sphere exactly). The constraint on reduced volume is enforced by setting the constraint area $\overline{A}$ to be the area of the original sphere-like shape, and setting the constraint volume $\overline{V}$ to be proportional to the original volume by factor v. Thus, for each simulation, the starting shape is in violation of the volume constraint, and is subject to a large pressure as defined by the penalized energy functional. The energy is then relaxed by conjugate gradient minimization and the resulting shapes and energies are compared to axisymmetric results from the literature. In order to achieve faster convergence of the nonlinear CG solver, the penalty coefficients μ_s and μ_v were chosen to produce somewhat "soft" constraints on area and volume, such that the computed area and volume combined to yield a reduced volume v which was accurate to within a factor of 10^{-3} of the desired value. The resulting energies are tabulated in Table 1, normalized by the energy of a spherical vesicle (with $v = 1$), $E_0 = 8\pi\mathscr{K}_C$.

For verification purposes, the finite element results are superposed over results obtained from integration of the axisymmetric Euler–Lagrange equations by Seifert [1] in Fig. 4. The figure clearly indicates agreement of the present results with those from the literature. One important feature revealed by Fig. 4 is the existence of multiple equilibrium shapes throughout the range of reduced volume. The three-dimensional equilibrium vesicle shapes corresponding to different reduced volumes are shown in Fig. 5, with each of the three different classes of equilibrium shapes (prolate, oblate, and stomatocyte) represented. Each of the simulations employed the same mesh (roughly spherical at initialization, as shown in Fig. 5(a)) made up of only 162 vertex nodes and 320 elements. Despite the relative coarseness of the meshes, the actual computational limit surfaces produced

Table 1
Vesicle energy as a function of reduced volume

v	1.0	0.9	0.8	0.65	0.58
$\frac{E}{8\pi\mathscr{K}_C}$	1.0	1.19	1.40	1.83	2.01

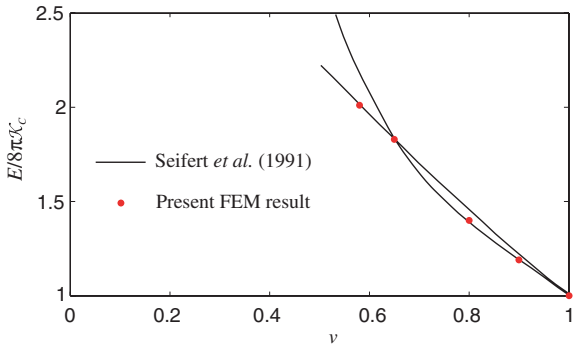

Fig. 4. Vesicle energy vs. reduced volume – comparison with axisymmetric results of Seifert et al. [10].

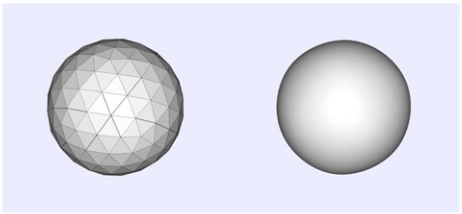

(a) Initial Shape, $v = 1.0$

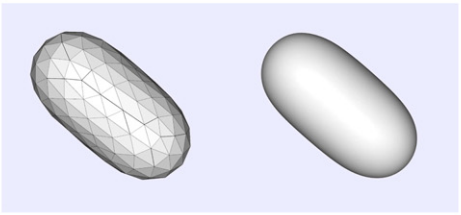

(b) $v = 0.9$

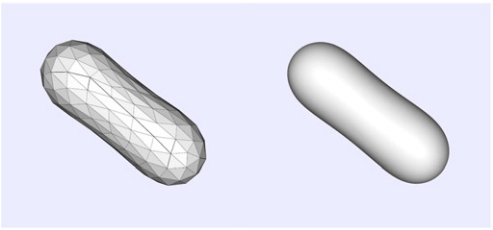

(c) $v = 0.8$

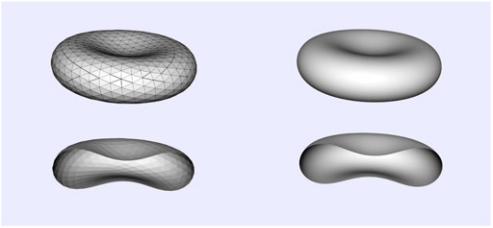

(d) $v = 0.65$

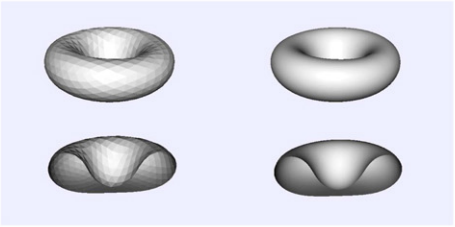

(e) $v = 0.58$

Fig. 5. Control meshes and limit surfaces of equilibrium shapes at various reduced volumes.

by the subdivision surface approximation basis functions are clearly quite smooth. The accuracy of the subdivision finite elements allows for the use of much coarser meshes than the finite-difference triangulation methods, which require more than an order of magnitude more vertices (e.g. 4000 in [18] and 2500 in [20]). This can yield a significantly smaller computational cost for the finite element approach over the finite difference methods. When the computational cost scales worse than linearly in the mesh size – as it does for Newton-type and conjugate gradient solution algorithms [33] – the relative efficiency of finite elements becomes even more noticable for finer meshes.

In the range $0.652 \leqslant v \leqslant 1$, both prolate (e.g. Figs. 5(b) and (c)) and oblate (e.g. Fig. 5(d)) shapes exist as stable equilibrium configurations, but the prolate shapes are global energy minimizers. At $v \approx 0.652$, a discontinuous oblate/prolate transition occurs and for small v oblates have lower energy than prolates. In addition, the dashed line tracks stomatocyte shapes (e.g. Fig. 5(e)) which appear below the oblate/stomatocyte transition at $v \approx 0.591$. It is noteworthy that the finite element simulations identified global energy minimizers at each chosen reduced volume, despite starting from a common sphere-like geometry. It is likely that equilibrium shapes in other portions of the phase diagram corresponding to local (but not global minimizers), such as the oblate curve over $0.652 \leqslant v \leqslant 1$, could be identified by "nudging" the conjugate gradient solver toward the desired shape with a judicious choice of initial geometry. In fact, it was observed in the simulations at lower reduced volume that the path of relaxation toward the minimum energy shape involved nonequilibrium transitions between the different axisymmetric shapes as well as other nonaxisymmetric shapes. Nonetheless, the ability of the solver to identify the global minima when not initialized with carefully chosen initial geometries can be viewed as encouraging evidence of the robustness of the present simulation framework.

5. Discussion

This paper has presented a framework for three-dimensional analysis of mechanics of lipid bilayer membranes/vesicles based on the finite element method. Within this framework C^1-conforming subdivision shell finite elements are employed for smooth parameterization of membrane surfaces, and the classic Canham–Helfrich–Evans curvature energy is minimized subject to constraints on surface area and enclosed volume. To validate the framework, equilibrium shapes have been simulated sampling points in the shape-phase diagram for varied reduced volumes.

Though the shapes resulting from these equilibrium calculations are axisymmetric, no assumption of axisymmetry is made *a priori*; on the contrary, the finite element framework is fully capable of computing nonaxisymmetric shapes as well. Of course, other methods are available for the calculation of nonaxisymmetric shapes, including finite-difference triangulation methods [17–20], global Ritz methods [15,16], PDE methods [22], and level set methods [24]. As demonstrated here, suitable accuracy can be obtained with meshes containing only hundreds of vertices, more than an order of magnitude fewer than required by finite-difference triangulation methods [18,20], which have garnered the largest popularity in the literature for nonaxisymmetric vesicle calculations. Global Ritz methods have been shown to attain suitable accuracy with about 100 modes, on the same order as the finite element method here. The PDE method of Bloor and Wilson [22] is significantly more efficient, requiring on the order of 5–10 basis functions.

Previous studies [28,29] have demonstrated the excellent convergence properties of the loop subdivision shell elements as compared to alternative shell element formulations in traditional engineering applications. Though it is reasonable to expect these results to apply in the present context as well, careful convergence studies comparing the performance of alternative finite element methods on bilayer problems remain to be done. This future work may lead to alternative techniques for dealing with spurious modes using mixed-C^0 or other element formulations.

In addition to its excellent accuracy, the finite element method also benefits from locality of approximation. In the current work, this feature is not utilized to its capacity; however, it is potentially quite useful, allowing for more natural simulation of complex forcing and geometric constraint scenarios. Application of generic local forces and boundary conditions can be extremely difficult with global approximation methods. Thus despite the computational efficiency of global Ritz, PDE, and level set methods, they are most appropriate for simulation of vesicles with only the simplest forces or geometric constraints applied (or none at all). Only the relatively inefficient finite-difference triangulation method shares the local properties of the finite element method. Locality can be extremely relevant, for example, when simulating vesicle adhesion or application of forces by micropipette and optical/magnetic tweezer techniques. Local methods also hold great potential for analysis of the increasingly voluminous library of geometric data obtained with cryo-electron microscopy (cryo-EM) and tomography (cryo-ET) techniques. Cryo-EM and -ET allow for direct experimental observation of three-dimensional membrane conformations in biologically relevant contexts. Their output is typically visualized by rendering membrane surfaces as triangulated meshes. Work is

presently underway on the development of techniques for extraction of mechanical force information from these data using finite difference and finite element frameworks. As another result of its locality, the finite element approximation offers promise for mechanics simulation of vesicles composed of multiple lipid types, modeling lipid concentration as a locally varying field. Some numerical work has focused on the Ginzburg–Landau and Cahn–Hilliard dynamcis of two-component bilayers using finite-difference triangulation [38] and Smooth Particle Applied Mechanics [39] methods. The finite element framework described here can be extended straightforwardly to model the two-component lipid system, using the energy minimization approach to complement previous studies of dynamics.

As discussed in Section 3.2, stabilization of tangential modes is key to the efficiency of the finite element method presented here. For the present calculations, local enforcement of the global area constraint and three-point numerical quadrature were shown to provide sufficient stabilization of zero-energy tangential dilatational modes for minimization with a nonlinear conjugate gradient algorithm. However, though minimization was achieved, the process was significantly slowed by the remaining zero-energy tangential shearing modes. Furthermore, it is plausible that the local area inextensibility may be overly restrictive for simulations involving larger deformations than those experienced in the simulations of Section 4. In other words, in certain contexts, the bilayer energy might be minimized more efficiently, by allowing the warpage of the mesh by ''flowing'' nodes out of regions of low curvature into regions of higher curvature. From this perspective, the lack of a reference configuration for the bilayer mesh can be seen as a feature to be used as an advantage. A virtual (i.e. physically meaningless) reference configuration can be used to introduce numerical forces and stiffness to rearrange and stabilize the finite element nodes tangentially on the surface without adversely affecting the energy landscape of the original membrane mechanics problem. Future work on such variational remeshing/regularization techniques will improve the effectiveness and efficiency of the finite element framework for simulation of more challenging bilayer mechanics problems.

Finally, the finite element framework is also naturally suited for analysis of the composite membranes of cells, in which the lipid bilayer is coupled mechanically to a cytoskeletal network. Indeed, for such a composite membrane, the cytoskeleton provides the local in-plane extensional and shear stiffnesses that are lacked by the fluid bilayer. In other words, the cytoskeleton behavior may be modeled more like a typical planar solid, parameterized by reference and deformed configurations. Thus the numerical instabilities observed for the pure bilayer vesicle are irrelevant for the composite membrane. Most theoretical models of cell deformation have focused on Hertzian analysis of the bulk elastic/viscoelastic behavior. However, the membrane can have an important mechanical effect [40]. Hence this finite element framework holds potential for future study of less-idealized composite cell membranes. Yet, even after extension of the framework for such membranes is complete, it is unlikely that the finite element approach will be the best choice for *every* membrane calculation. Clearly, other existing methods are now and may remain superior in some cases (e.g. [22] for computing unloaded equilibrium shapes, and [23,24] for simulating topological changes). Nevertheless, the advantages of finite element approach make it a generally useful tool for probing the fascinating and challenging problems of lipid bilayer membrane mechanics.

Acknowledgments

The authors are grateful to Erich Sackmann for sharing with us many insights on bilayer mechanics as well as suggestions for future work. Paul Wiggins, Eric Peterson, Rob Phillips, Mathias Jungen, Kaushik Bhattacharya, and Michael Ortiz have each made valuable suggestions as well. The authors thank the reviewers for their helpful comments and suggestions.

References

[1] U. Seifert, Configurations of fluid membranes and vesicles, Adv. Phys. 46 (1) (1997) 13–137.
[2] H.T. McMahon, J.L. Gallop, Membrane curvature and mechanisms of dynamic cell membrane remodelling, Nature 428 (2005) 590–596.
[3] J.R. McIntosh, Electron microscopy of cells: a new beginning for a new century, J. Cell Biol. 153 (6) (2001) F25–F32.
[4] T.G. Frey, C.A. Mannella, The internal structure of mitochondria, Trends Biochem. Sci. 25 (7) (2000) 319–324.

[5] P.B. Canham, The minimum energy of bending as a possible explanation of the biconcave shape of the red blood cell, J. Theor. Biol. 26 (1970) 61–81.
[6] W. Helfrich, Elastic properties of lipid bilayers: theory and possible experiments, Z. Naturforsch. C 28 (1974) 693–703.
[7] E.A. Evans, Bending resistance and chemically induced moments in membrane bilayers, Biophys. J. 14 (12) (1974) 923–931.
[8] J.T. Jenkins, Static equilibrium configurations of a model red blood cell, J. Math. Biol. 4 (1977) 149–169.
[9] J.T. Jenkins, The equations of mechanical equilibrium of a model membrane, SIAM J. Appl. Math. 32 (4) (1977) 755–764.
[10] U. Seifert, K. Berndl, R. Lipowsky, Shape transformations of vesicles-phase-diagram for spontaneous-curvature and bilayer-coupling models, Phys. Rev. A 44 (1991) 1182–1202.
[11] U. Seifert, Shape transformation and free, toroidal and bound vesicles, J. Phys. Colloque 51 (C7) (1990) 339–344.
[12] W. Wiese, W. Harbich, W. Helfrich, Budding of lipid bilayer vesicles and flat membranes, J. Phys.: Condens. Matter 4 (1992) 1647–1657.
[13] B. Bozic, S. Svetina, B. Zeks, R.E. Waugh, Role of lamellar membrane structure in tether formation from bilayer vesicles, Biophys. J. 61 (1992) 963–973.
[14] L. Miao, U. Seifert, M. Wortis, H.G. Döbreiner, Budding transitions of fluid-bilayer vesicles: the effect of area difference elasticity, Phys. Rev. E 49 (1994) 5389–5407.
[15] V. Heinrich, B. Božič, S. Saša, B. Žekš, Vesicle deformation by an axial load: from elongated shapes to tethered vesicles, Biophys. J. 76 (1999) 2056–2071.
[16] V. Heinrich, S. Sǎsa, B. Žekš, Nonaxisymmetric vesicle shapes in a generalized bilayer-couple model and the transition between oblate and prolate axisymmetric shapes, Phys. Rev. E 48 (4) (1993) 3112–3123.
[17] L. Hsu, R. Kusner, J. Sullivan, Minimizing the squared mean curvature integral for surfaces in space forms, Exp. Math. 1 (3) (1992) 191–207.
[18] M. Jaric, U. Seifert, W. Wintz, M. Wortis, Vesicular instabilities: the prolate-to-oblate transition and other shape instabilities of fluid bilayer membranes, Phys. Rev. Lett. 52 (1995) 6623.
[19] M. Kraus, U. Seifert, R. Lipowsky, Gravity-induced shape transformations of vesicles, Europhys. Lett. 32 (5) (1995) 431–436.
[20] W. Wintz, H.-H. Döbereiner, U. Seifert, Starfish vesicles, Europhys. Lett. 33 (1996) 403–408.
[21] K.A. Brakke, The surface evolver, Exp. Math. 1 (2) (1992) 141–165.
[22] M.I.G. Bloor, M.J. Wilson, Method for efficient shape parametrization of fluid membranes and vesicles, Phys. Rev. E 61 (4) (2000) 4218–4229.
[23] Q. Du, C. Liu, X. Wang, A phase field approach in the numerical study of the elastic bending energy for vesicle membranes, J. Comput. Phys. 198 (2004) 450–468.
[24] Q. Du, C. Liu, X. Wang, Simulating the deformation of vesicle membranes under elastic bending energy in three dimensions, J. Comput. Phys. 212 (2) (2006) 757–777.
[25] O.C. Zienkiewicz, R.L. Taylor, The Finite Element Method, vols. 1–3, Butterworth-Heinemann, Oxford, 2000.
[26] M. Dao, C.T. Lim, S. Suresh, Mechanics of the human red blood cell deformed by optical tweezers, J. Mech. Phys. Solids 51 (2003) 2259–2280.
[27] W.G. Strang, G.J. Fix, An Analysis of the Finite Element Method, Wellesley Cambridge Press, 1973.
[28] F. Cirak, M. Ortiz, P. Schröder, Subdivision surfaces: a new paradigm for thin-shell finite-element analysis, Int. J. Numer. Methods Eng. 47 (2000) 2039–2072.
[29] F. Cirak, M. Ortiz, Fully C^1-conforming subdivision elements for finite element-deformation thin-shell analysis, Int. J. Numer. Methods Eng. 51 (2001) 813–833.
[30] I.S. Sokolnikoff, Tensor Analysis: Theory and Applications to Geometry and Mechanics of Continua, second ed., Wiley, New York, 1964.
[31] M. Do Carmo, Differential Geometry of Curves and Surfaces, Prentice Hall, 1976.
[32] D.G. Luenberger, Linear and Nonlinear Programming, Addison-Wesley, 1989.
[33] J. Nocedal, S. Wright, Numerical Optimization, Springer, 1999.
[34] R. Capovilla, J. Guven, J.A. Santiago, Deformations of the geometry of lipid vesicles, J. Phys. A: Math. Gen. 36 (2003) 6281–6295.
[35] J. Warren, Subdivision Methods for Geometric Design: A Constructive Approach, Elsevier Science and Technology Books, 2001.
[36] C. Loop, Subdivision surfaces based on triangles, Master's thesis, University of Utah, Department of Mathematics, 1987.
[37] F. Jürlicher, U. Seifert, R. Lipowsky, Conformal degeneracy and conformal diffusion of vesicles, Phys. Rev. Lett. 71 (1993) 452–455.
[38] T. Taniguchi, Shape deformation and phase separation dynamics of two-component vesicles, Phys. Rev. Lett. 76 (23) (1996) 4444–4447.
[39] G.S. Ayton, J.L. McWhirter, P. McMurtry, G.A. Voth, Coupling field theory with continuum mechanics: a simulation of domain formation in giant unilamellar vesicles, Biophys. J. 88 (6) (2005) 3855–3869.
[40] S. Sen, S. Subramanian, D.E. Discher, Indentation and adhesive probing of a cell membrane with AFM: theoretical model and experiments, Biophys. J. 89 (2005) 3203–3213.